Available online at www.sciencedirect.com
SCIENCE DIRECT®
Sensors and Actuators B 89 (2003) 315–323
SENSORS AND ACTUATORS B CHEMICAL
www.elsevier.com/locate/sensorb

Monolithic membrane valves and diaphragm pumps for practical large-scale integration into glass microfluidic devices

William H. Grover[a], Alison M. Skelley[a], Chung N. Liu[b], Eric T. Lagally[c], Richard A. Mathies[a,c,*]

[a]Department of Chemistry, University of California, Berkeley, CA 94720, USA
[b]Department of Chemical Engineering, University of California, Berkeley, CA 94720, USA
[c]UC Berkeley/UC San Francisco Joint Bioengineering Graduate Group, University of California, Berkeley, CA 94720, USA

Accepted 11 December 2002

Abstract

Monolithic elastomer membrane valves and diaphragm pumps suitable for large-scale integration into glass microfluidic analysis devices are fabricated and characterized. Valves and pumps are fabricated by sandwiching an elastomer membrane between etched glass fluidic channel and manifold wafers. A three-layer valve and pump design features simple non-thermal device bonding and a hybrid glass-PDMS fluidic channel; a four-layer structure includes a glass fluidic system with minimal fluid-elastomer contact for improved chemical and biochemical compatibility. The pneumatically actuated valves have <10 nl dead volumes, can be fabricated in dense arrays, and can be addressed in parallel via an integrated manifold. The membrane valves provide flow rates up to 380 nl/s at 30 kPa driving pressure and seal reliably against fluid pressures as high as 75 kPa. The diaphragm pumps are self-priming, pump from a few nanoliters to a few microliters per cycle at overall rates from 1 to over 100 nl/s, and can reliably pump against 42 kPa pressure heads. These valves and pumps provide a facile and reliable integrated technology for fluid manipulation in complex glass microfluidic and electrophoretic analysis devices.

Keywords: PDMS membrane valves; Micropumps; Integrated devices

1. Introduction

Microfluidic lab-on-a-chip analyzers have advanced rapidly from early single-channel devices [1] to current complex systems that can perform a wide variety of assays [2,3]. Successful microfluidic assays have included polymorphism detection for breast cancer risk assessment [4], parallel combinatorial synthesis and analysis of chemical libraries [5], high-throughput genotyping [6] and DNA sequencing [7], chemical and biological antigen detection [8], and chiral resolution of amino acids for exobiological analysis [9]. However, the development of complete integrated systems for on-chip sample preparation and manipulation has shown more modest growth. Thus far, automated HIV genotyping has been demonstrated in a polymer microfluidic device that combines purification, amplification, and microarray hybridization steps [10], DNA amplification and integrated electrophoretic analysis in a glass microfluidic device has been demonstrated using individually addressed valves and vents to isolate fluids [11], automated protein sizing has been performed in a glass device using pressure-driven flow and electrophoresis to route fluids [12], and automated pathogen detection has been demonstrated in a micromachined polymer device utilizing membrane valves and pumps [13]. Complex fabrication, chemical compatibility, and unreliable fluid manipulation, among other problems, have made existing fluidic manipulation technologies disadvantageous for integration into large-scale, high-throughput lab-on-a-chip devices. A useful on-chip mechanism for nl- to μl-scale fluid manipulation must be compatible with the assay chemistry, be able to accurately and reliably meter known volumes of fluid, and be amenable to facile large-scale integration.

A variety of microfabricated valves and pumps have been developed for on-chip fluidic manipulation and control. The earliest examples were fabricated using anodically bonded silicon and glass wafers and actuated piezoelectrically [14,15]. The electrical conductivity and chemical compatibility of silicon, which can complicate its use in analytical

* Corresponding author. Tel.: +1-510-642-4192; fax: +1-510-642-3599.
E-mail address: rich@zinc.cchem.berkeley.edu (R.A. Mathies).

0925-4005/03/$ – see front matter © 2003 Elsevier Science B.V. All rights reserved.
doi:10.1016/S0925-4005(02)00468-9

devices, can be mitigated in part by the use of deposited chemically and electrically resistant thin films [16]. Flexible membranes can also be used to form the active elements in pneumatically actuated microfluidic valves and pumps. A variety of membrane-based valves and pumps have been demonstrated for silicon [17–19], glass–silicon [20,21], and polymer [10,22–24] microfluidic devices. In addition, the popularity of "soft lithography" [25] has led to the development of pneumatic valves and pumps suitable for integration into all-elastomer devices [26,27]. While these demonstrations of elastomeric valves and pumps are encouraging, the hydrophobicity and porosity of many native elastomer surfaces render these valves and pumps incompatible with many chemical and biochemical assays unless surface modification chemistries are employed [28,29]. Also, while successful fluorescence detection in an elastomer device has been demonstrated [30,31], the native fluorescence of elastomeric material under visible light is significantly higher than that of glass.[1] This presents a problem for our applications that demand high sensitivity detection. Finally, a variety of pumping methods based on electroosmotic flow (EOF) have been demonstrated [32–34]. These methods are useful for many applications although the sensitivity of EOF to analyte osmotic strength and surface contamination must be noted.

Glass microfluidic devices [1] have dominated applications where precise control of the fluidic channel surface chemistry, high quality electrophoretic separation, and high-sensitivity fluorescence detection are required. The variety of glass silanization chemistries [35] coupled with the insulating nature of glass make it particularly well-suited for use in capillary electrophoresis (CE) analysis devices [36]. The success of pneumatically actuated valves for polymer microfluidic devices [10] inspired the development of a pneumatic valve suitable for integration into glass analytical devices [37]. While this valve has been used successfully in a variety of glass CE devices [11,38,39], its reliance on individually placed latex membranes is problematic for large-scale integration into high-throughput devices.

Here we present the fabrication and characterization of membrane valves and diaphragm pumps that can be used for facile large-scale integration into glass microfluidic analysis devices. The valves and pumps employ a monolithic polydimethylsiloxane (PDMS) elastomer membrane, an integrated microfabricated manifold that provides independent addressing or parallel pneumatic actuation of arrays of valves and pumps, and a glass fluidic system that minimizes fluid-elastomer contact.[2] The ease of fabrication and reliability of these valves and pumps will facilitate the development of high-throughput glass microfluidic devices.

[1] A sample of PDMS membrane used in this study was found to be over thirty times more fluorescent than an equal thickness of borosilicate glass. The samples were illuminated at 488 nm; emitted light from 535 to 565 nm was collected through a band pass filter and detected using a CCD camera.

[2] A preliminary presentation of this work is found in [40].

2. Materials and methods

2.1. Microfabrication

The three- and four-layer device topologies used to fabricate monolithic membrane valves and pumps are illustrated in Fig. 1. Channel features were etched into glass wafers using standard wet chemical etching [36,38]. Glass

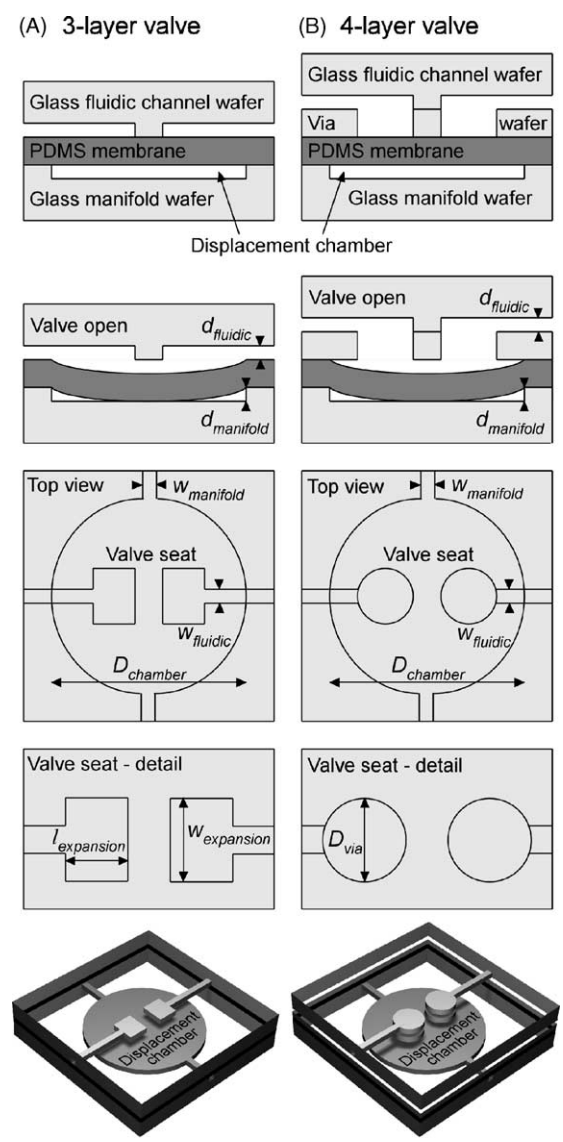

Fig. 1. Cross-sectional, top, and oblique views of three-layer (A) and four-layer (B) monolithic PDMS membrane valves. Each valve consists of a glass manifold with an etched displacement chamber for pneumatic actuation, a working PDMS membrane, and a glass fluidic channel wafer containing the channel to be valved. In the three-layer topology, PDMS defines one surface of the valved channel. In the four-layer structure, the addition of the drilled via wafer defines all-glass fluidic channels with minimal fluid-PMDS contact. The three-layer valve includes a channel expansion in the valve seat with dimensions $w_{expansion}$ by $l_{expansion}$, while the four-layer valve includes drilled via holes with diameter D_{via}. The wafer etch depths are $d_{fluidic}$ and $d_{manifold}$, channel widths are $w_{fluidic}$ and $w_{manifold}$, and displacement chamber diameter is $D_{chamber}$.

wafers (1.1 mm thick, 100 mm diameter) were piranha cleaned (20:1 H_2SO_4:H_2O_2) and coated with a sacrificial 200 nm polysilicon layer using an LPCVD furnace or sputtering system. Borofloat glass wafers were used for devices with the three-layer design and D263 borosilicate glass wafers were used for devices with the four-layer design. After polysilicon deposition, the wafers were spin-coated with positive photoresist, soft-baked, and patterned using a contact aligner. UV-exposed regions of photoresist were removed in Microposit developer. The exposed regions of polysilicon were removed by etching in SF_6 plasma. The wafers were etched isotropically at 7 μm/min in HF solution (49% HF for the Borofloat wafers and 1:1:2 HF:HCl:H_2O for the D263 wafers) until the desired etch depth was reached. The fluidic channel wafers were etched 20 μm deep for the three-layer devices and 40 μm deep for the four-layer devices. The manifold wafers were etched 70 μm deep for the three-layer devices and drilled at valve locations for the four-layer devices. The remaining photoresist and polysilicon was then stripped from the wafers using PRS-3000 and SF_6 plasma, respectively. Access holes through the fluidic and manifold wafers were drilled and the wafers were again piranha cleaned.

Devices utilizing the three-layer design shown in Fig. 1A were assembled by applying a PDMS (polydimethylsiloxane) membrane (254 μm thick HT-6135 and HT-6240, Bisco Silicones, Elk Grove, IL) over the etched features in the fluidic channel wafer and pressing the manifold wafer onto the PDMS membrane. This process formed hybrid glass-PDMS fluidic channels with valves located wherever a drilled or etched displacement chamber on the manifold was oriented directly across the PDMS membrane from a valve seat. Devices utilizing the four-layer design in Fig. 1B were assembled by first thermally bonding the fluidic channel wafer to a 210 μm thick D263 via wafer with pairs of 254 μm diameter drilled via holes positioned to correspond to the locations of channel gaps. The fluidic channel and via wafers were bonded by heating at 570 °C for 3.5 h in a vacuum furnace (J.M. Ney, Yucaipa, CA). The resulting two-layer structure containing all-glass channels was then bonded to the PDMS membrane and the manifold wafer as described above. The glass-PDMS bonds formed in this manner were reversible but still strong enough to survive the range of vacuum and pressures exerted on the device. Optionally, an irreversible glass-PDMS bond was obtained by cleaning the manifold wafer and PDMS membrane in a UV ozone cleaner (Jelight Company Inc., Irvine, CA) immediately prior to assembly.

2.2. Operation and characterization

The monolithic membrane valves with integrated manifolds were actuated by vacuum or pressure applied to pneumatic connections on the device and distributed by the channels in the manifold wafer to the displacement chambers. Similarly, monolithic membrane valves without integrated manifolds were actuated by applying vacuum or pressure directly to drilled displacement chambers on the manifold wafer beneath each valve. Applying a vacuum deflected the PDMS membrane into the displacement chambers, thereby allowing fluid to flow across the gaps in the fluid channels. Applying pressure forced the PMDS membrane against the fluidic channel wafer, thereby stopping the flow of fluid. Valve actuation was found to occur in two steps, with only the regions of membrane directly below the fluid channels deflecting at first, then the remainder of the membrane separating from the valve seat on the fluidic channel wafer and deflecting into the displacement chamber as the valve opened fully. Expanding the end of the fluidic channel within the valve seat was found to decrease the pressure differential required to initiate the first step in valve actuation. For this reason, expanded fluidic channels were included in all valves used in this study. Pressure and vacuum for valve actuation were controlled by a set of solenoid valves (Humphrey Products, Kalamazoo, MI) and a computer running LabVIEW (National Instruments, Austin, TX); measurements of actuation pressure or vacuum were relative to atmospheric.

Three valves placed in series form a diaphragm pump, as shown in Fig. 2. The three-layer diaphragm pump test wafer shown in Fig. 2 contains 144 valves configured to form 48 different pumps. Pumping was realized by actuating the input, diaphragm, and output valves of each pump according to the five-step cycle shown in Fig. 3. The 48 pumps in the test device were actuated in parallel via three sets of

Table 1
Diaphragm pump dimensions

Pump	$D_{chamber}$ (μm)[a]	$V_{chamber}$ (nl)[b]
1	1000	67.1
2	1250	101
3	1500	142
4	1750	198
5	2000	244
6	2250	306
7	2500	374
8	2750	449
9	3000	531
10	4000	928
11	5000	1430
12	6000	2050
	$w_{fluidic}$ (μm)[c]	$A_{fluidic}$ (μm^2)[d]
25	300	6630
28	240	5430
30	200	4630
33	140	3430
35	100	2630
38	40	1430

[a] Displacement chamber diameter.
[b] Etched displacement chamber volume.
[c] Fluidic channel width.
[d] Etched fluidic channel cross-sectional area.

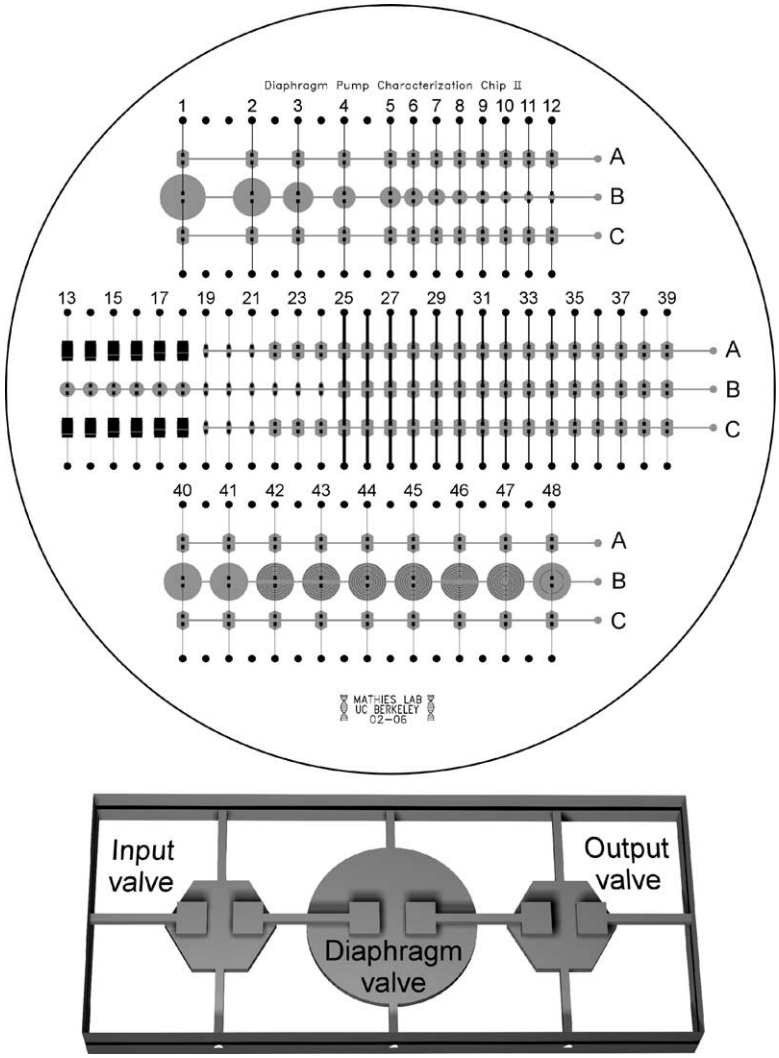

Fig. 2. Three-layer diaphragm pump characterization wafer. The wafer contains 144 valves arranged to form 48 different pumps; critical dimensions of the pumps are summarized in Table 1. Pneumatic connections at drilled holes A, B, and C are used to actuate each series of pumps in parallel. Pumps 40 through 48 were designed to test different valve seat fluidic channel geometries. Pumps with meandering or interdigitated fluidic channels in the valve seats (pumps 42 through 48) were found to be more resistant to bubble entrapment and pump more reliably than pumps with standard valve seats (pumps 40 and 41). Inset shows an oblique view of one pump.

three pneumatic connections (A, B, and C in Fig. 2) on the underside (manifold wafer) of the device.

The dependence of pump performance on diaphragm valve displacement chamber volume was characterized using pumps 1 through 12. The pre-etch diaphragm valve displacement chamber diameter D_{chamber} and post-etch chamber volume V_{chamber} for pumps 1 through 12 are summarized in Table 1. V_{chamber} was calculated using an isotropic etch model

$$V_{\text{chamber}} = \tfrac{1}{4}\pi D_{\text{chamber}}^2 d_{\text{manifold}} + \tfrac{1}{4}\pi^2 D_{\text{chamber}} d_{\text{manifold}}^2.$$

The identical input and output valves utilized 1.6 mm × 1.8 mm hexagonal displacement chambers with chamber volume $V_{\text{chamber}} = 270$ nl. The input, diaphragm, and output valves in pumps 1 through 12 had identical fluidic channel expansions ($w_{\text{expansion}} = 300$ μm, $l_{\text{expansion}} = 500$ μm) separated by a 500 μm gap.

The dependence of pump performance on fluidic channel cross-sectional area was characterized using pumps 25, 28, 30, 33, 35, and 38. The pre-etch fluidic channel width w_{fluidic} and post-etch channel cross-sectional area A_{fluidic} for the six pumps are reported in Table 1. A_{fluidic} was calculated using an isotropic etch model

$$A_{\text{fluidic}} = w_{\text{fludic}} d_{\text{fluidic}} + \tfrac{1}{2}\pi d_{\text{fluidic}}^2.$$

Pumps 25, 28, 30, 33, 35, and 38 had identical input, output, and diaphragm valves consisting of 1.6 mm × 1.8 mm hexagonal displacement chambers with chamber volume $V_{\text{chamber}} = 270$ nl, $w_{\text{expansion}} = 300$ μm, $l_{\text{expansion}} = 500$ μm separated by a 500 μm gap.

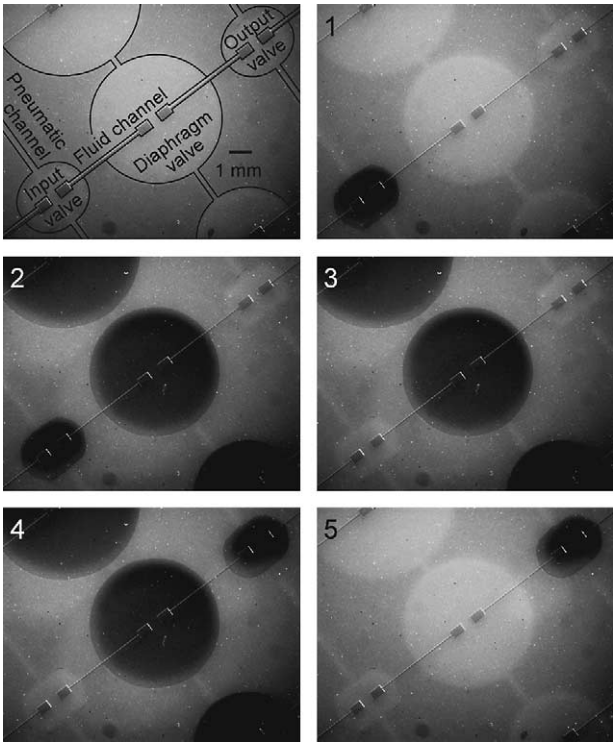

Fig. 3. Darkfield images showing the five steps in the diaphragm pumping cycle: (1) open input valve and close output valve, (2) open diaphragm valve, (3) close input valve, thereby defining the volume pumped per cycle as the volume contained within the open diaphragm valve, (4) open output valve, (5) close diaphragm valve.

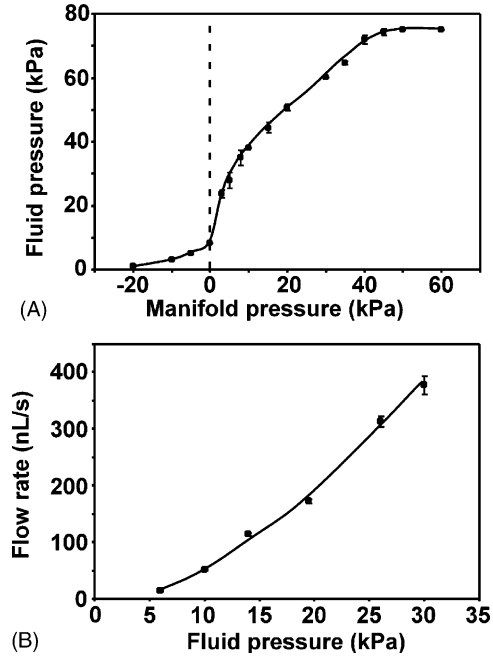

Fig. 4. (A) Fluid pressure required to initiate water flow through a valve being held at the indicated manifold pressure. (B) Flow rate of water through a valve as a function of pressure applied to the fluid while holding the valve open with a constant vacuum of −30 kPa. A four-layer valve with a HT-6240 PDMS membrane was used. Valve dimensions were $d_{fluidic} = 40$ μm, $d_{manifold} = 1100$ μm, $w_{fluidic} = 100$ μm, $D_{via} = 254$ μm, and $D_{chamber} = 1500$ μm. The calculated dead volume of the valve (based on the volume of the two drilled via holes) was 20 nl; three-layer monolithic membrane valves with similar dimensions had 8 nl calculated dead volumes.

3. Results

3.1. Valve characterization

Fig. 4A presents a characterization of water flow through a four-layer monolithic membrane valve. The valve offered very little resistance to fluid flow at manifold pressures below 0 kPa. Increasing the manifold pressure at the PDMS membrane quickly increased the amount of pressure required to break fluid through the channel gap. Applying a manifold pressure of only 10 kPa effectively sealed the valve against 40 kPa fluid pressure, and a manifold pressure of 45 kPa sealed the valve against fluid pressures as high as 75 kPa. Acting over a membrane surface area of 50,000 μm^2, the 75 kPa fluid pressure exerted a force of 3.8 mN on the membrane. The manifold pressure acted over a much larger section of membrane (1.8 mm^2) but the flexible membrane applied most of this force to the wafer and only a fraction of the net manifold force actively counteracted the fluid force. Still, the valve sealed successfully against a fluid pressure nearly double the manifold pressure, and valves with thicker or less elastic membranes would be expected to hold off even greater fluid pressures at the same manifold pressure.

Fig. 4B presents the rate of water flow through an open monolithic membrane valve as a function of applied fluid pressure. The rate of fluid flow through the valve was found to have a roughly linear dependence upon the fluid pressure, and flow rates as high as 380 nl/s were attainable for the valve tested. The initial resistance to flow between 0 and 5 kPa fluid pressure was attributed to the hydrophobic nature of the PDMS membrane. For this and other three- and four-layer valves with fluidic channel cross-sectional areas ($A_{fluidic}$) much smaller than the cross-sectional area of the fluid path through the open valve, the overall rate of fluid flow is primarily determined by $A_{fluidic}$.

3.2. Diaphragm pump characterization

The 48-pump device shown in Fig. 2 was used to characterize the performance of diaphragm pumps constructed from monolithic membrane valves. Fig. 5 plots the maximum volume pumped per cycle versus the displacement chamber volume $V_{chamber}$ of the diaphragm (central) valve for pumps 1 through 12 at zero pressure head. All five steps in the pumping cycle were given excess time to occur (1.5 s for steps 1, 3, and 4 and up to 10 s for steps 2 and 5) to ensure that all valves had ample time to open and close fully and to maximize the volume pumped per cycle. The linear correlation shows that the maximum volume pumped per cycle is directly dependent upon $V_{chamber}$, with approximately 82%

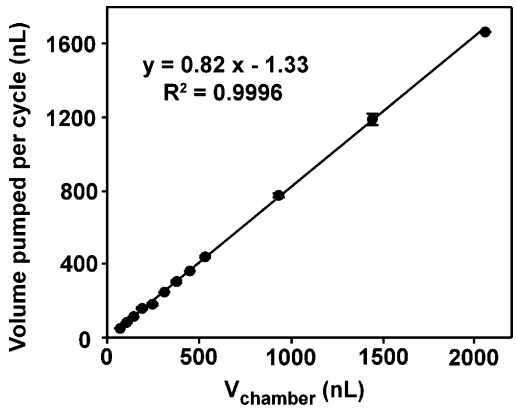

Fig. 5. Maximum volume of water pumped per cycle as a function of the diaphragm valve chamber volume for pumps 1 through 12. Valve actuation vacuum and pressure were −80 and 40 kPa, respectively. A three-layer device with a 20 μm etch depth fluid layer, 70 μm etch depth manifold layer, and 254 μm thick HT-6135 PDMS membrane was used. Diaphragm valve displacement chamber dimensions are presented in Table 1; the input and output valves of each pump were held constant at $V_{chamber} = 274$ nl. For all valves, $w_{expansion} = 300$ μm, $l_{expansion} = 500$ μm, and the gap was 500 μm.

of $V_{chamber}$ pumped per cycle. This relationship between volume pumped per cycle and displacement chamber volume enables the design of pumps for metering precisely known volumes.

Fig. 6 explores the relationship between diaphragm valve actuation time and volume pumped per cycle for pumps 1 through 12 at zero pressure head. The optimal diaphragm actuation time of each pump was determined by holding cycle steps 1, 3, and 4 at an excess actuation time of 1.5 s each and varying the actuation time of the diaphragm valve (steps 2 and 5) until a maximum pumping rate was reached. The optimal diaphragm valve actuation time was found to be a linear function of the volume pumped per cycle, indicating that regardless of pump size, diaphragm valve emptying (the actual "pumping step" in the cycle) occurred at a constant rate of 260 nl/s determined from the reciprocal of the slope of the linear regression. A constant fluid flow rate is expected in a system with constant pressure (the 40 kPa valve actuation pressure) forcing fluid through a channel with constant cross-sectional area ($A_{fluidic} = 1030$ μm^2); our data clearly fit this expectation.

Fig. 6 also explores the maximum pumping rate attainable for each pump at zero pressure head. At the smallest volume pumped per cycle (pump 12), only 300 ms of the total 5.1 s cycle (6%) was spent emptying the diaphragm valve and the overall pumping rate was only 10 nl/s. At the largest volume pumped per cycle (pump 1), 6.5 s of the total 17.5 s cycle (37%) was used for closing the diaphragm valve and the pumping rate rose to 89 nl/s. To pump at this rate, the diaphragm valve emptied at an overall rate of 240 nl/s. This value is close to the 260 nl/s maximum measured earlier and indicates that the pump operation is indeed optimized. Other results indicate that reducing the actuation times for steps 1, 3, and 4 (which were kept excessively long for the purposes of this figure) increases both the fraction of the cycle devoted to diaphragm emptying and the overall pumping rate. Also, since smaller valves require shorter actuation times and $V_{chamber}$ of the input and output valves does not have a direct effect on the volume pumped per cycle, minimizing $V_{chamber}$ of the input and output valves further increases the overall pumping rate.

Fig. 7 explores the effect of fluidic channel cross-sectional area $A_{fluidic}$ on the optimal cycle time using pumps 25, 28, 30, 33, 35, and 38. The optimal cycle time of each pump was found by setting all five cycle steps to the same time and varying this time until a maximum pumping rate was reached. The inverse second-order polynomial relationship between optimal pump cycle time and $A_{fluidic}$ is in agreement with Poiseuille's law using a constant pressure to force a constant volume of fluid through cylindrical channels of different cross-sectional areas. Fig. 7 also shows the maximum pumping rate for pumps 25, 28, 30, 33, 35, and 38.

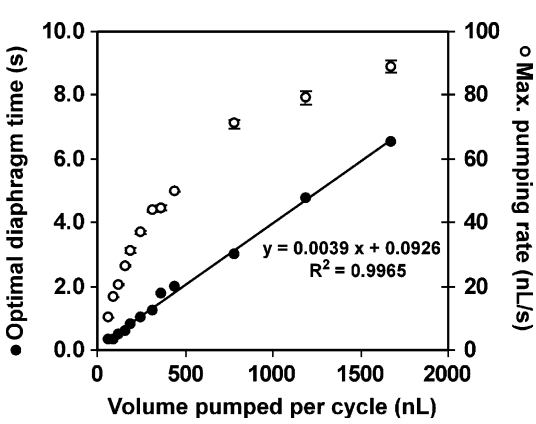

Fig. 6. Optimal diaphragm actuation time (●) and maximum pumping rate (○) as functions of volumes of water pumped per cycle for pumps 1 through 12. Device parameters were the same as in Fig. 5.

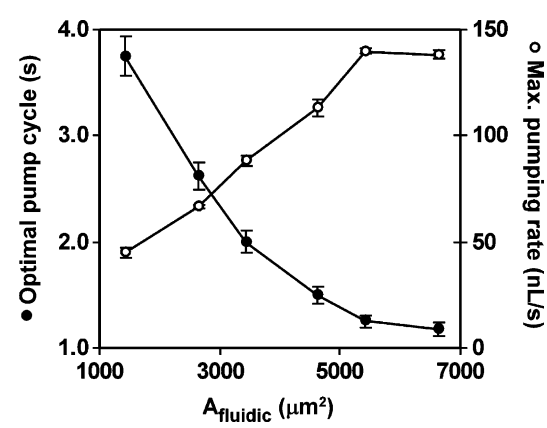

Fig. 7. Optimal pump cycle time (●) and maximum water pumping rate (○) as functions of $A_{fluidic}$ for pumps 25, 28, 30, 33, 35, and 38. Valve actuation vacuum and pressure were −80 and 40 kPa, respectively. Channel cross-sectional areas are presented in Table 1; other device parameters were the same as in Fig. 5.

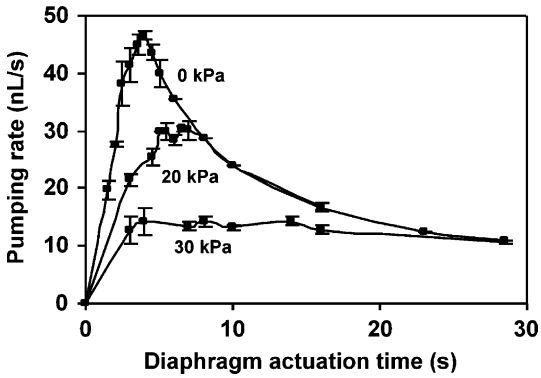

Fig. 8. Pumping rates attainable at three different pressure heads as functions of diaphragm valve actuation time. Pump 3 on a three-layer device with a 20 μm etch depth fluid layer, 70 μm etch depth manifold layer, and 254 μm thick HT-6240 PDMS membrane was used. Valve actuation vacuum and pressure were −80 and 40 kPa, respectively.

The maximum pumping rate attainable rises as a roughly linear function of the fluid channel cross-sectional area until a maximum pumping rate of approximately 140 nl/s is reached. This plateau is likely due to the fast cycle rate coupled with the finite amount of time required to pressurize and depressurize the pneumatic control system. This relationship between fluidic channel cross-sectional area and maximum pumping rate makes pumps designed for specific pumping rates possible.

Finally, Fig. 8 explores the effect of cycle time for pumping water against various regulated pressure heads at the output. Pumping rate data were obtained at pressure heads of 0, 20, and 30 kPa using pump 3 in Fig. 2. Only diaphragm valve actuation times (steps 2 and 5) were varied; input and output valve actuation times (steps 1, 3, and 4) were held at a constant dwell time of 1.5 s each. At 0 kPa pressure head, a clear maximum pumping rate of 47 nl/s was reached at a diaphragm actuation time of 5 s. This maximum pumping rate is lower than the 70 nl/s measured for this pump in Fig. 6 because of the decreased elasticity of the HT-6240 membrane (250% elongation) compared to the HT-6135 membrane (450% elongation) used in prior pump characterizations. These and other results indicate that identical pumps fabricated with thicker or less-elastic PDMS membranes consistently pump a smaller fraction of $V_{chamber}$ per cycle because the membrane fills less of the displacement chamber and translates less of $V_{chamber}$ to the fluidic wafer, and pumps fabricated with thinner or more-elastic membranes pump a larger fraction of $V_{chamber}$ per cycle as the membrane fills more of the displacement chamber. Applying a pressure head decreased the maximum pumping rate, with 30 nl/s attainable at 20 kPa pressure head and 13 nl/s attainable at 30 kPa pressure head. Pumping rates at all three pressure heads converge when diaphragm valve actuation times are used that exceed the time required for complete closure of the diaphragm valve. While pumping rates decreased with applied fluid pressure, reliable pumping was attainable at fairly high pressure heads. In a related study, the maximum reachable pressure at blocked flow was measured by blocking the output of a diaphragm pump and actuating the pump until the output pressure reached a constant. As expected, the output pressure was found to asymptotically approach the pump actuation pressure, with 42 kPa output pressure attainable using a 43 kPa actuation pressure.

4. Discussion and conclusions

The monolithic valves and pumps developed and evaluated here have a number of advantages for nl- and μl-scale fluid manipulation. Monolithic membrane valves are "normally closed" and require no manifold pressure when sealing against the negligible fluid pressures commonly encountered in many microfluidic devices. Devices utilizing "normally open" pneumatic valves [27] cannot be depressurized without losing control of the fluid contents. The monolithic membrane valves presented here are larger than some pneumatic valves in the literature [26,27] and provide a relatively large active area for actuation pressure and vacuum. This decreases the magnitude of pressure and vacuum required to actuate the valves and increases the maximum fluid pressure against which the valves seal without failure: 10 kPa manifold pressure seals the monolithic membrane valves against fluid pressures up to 40 kPa, and −20 kPa manifold vacuum is adequate to fully open the valve. While smaller pneumatic valves can be fabricated in denser arrays and actuated more rapidly, they require greater pressures [27] or vacuums [26] for reliable actuation. The four-layer monolithic membrane valves contribute 20 nl dead volume and the smallest three-layer valves contribute only 8 nl dead volume; these volumes are an order of magnitude smaller than the analyte volumes commonly encountered in many current microfluidic bioassays [11,39]. The use of commercially available elastomer membranes in the valves and pumps simplifies and expedites device fabrication. The monolithic membrane diaphragm pumps have been demonstrated to pump reliably at a variety of pumping rates and pressure heads. They are self-priming and pump fluids forward or backward simply by reversing the actuation cycle. Indeed, any number of input/output valves may be connected to a single diaphragm valve to construct a multidirectional fluidic router. The integrated microfabricated manifold like that used in all-elastomer devices [26,27] allows for monolithic membrane valve and pump placement at any point on the analysis device and actuation of arrays of pumps or valves in parallel. Finally, by adjusting the volume of the diaphragm valve displacement chamber, the volume pumped per actuation may be determined at the fabrication stage. Diaphragm pumps may therefore be used to meter nanoliters to microliters of fluid in applications that require precise control of fluid volumes and fluid position within a device.

In conclusion, reliable microvalves and micropumps suitable for large-scale integration into glass chemical

and biochemical assay devices have been fabricated and characterized. Facile microfabrication coupled with an integrated manifold make massively parallel actuation of arrays of valves and pumps possible for the first time in glass microfluidic devices. In addition, the four-layer valve and pump design incorporates an all-glass fluidic system to minimize fluid-PDMS contact for improved chemical compatibility. Systematic analysis of dimensions and actuation conditions shows that valves and pumps with specific operational characteristics can be easily designed and fabricated. The simplicity of large-scale monolithic valve and pump fabrication coupled with the chemical compatibility of the glass microfluidic analysis platform make these valves and pumps well suited for integration into bioassay devices. For example, this work will be critical in the development of arrays of PCR-CE integrated microdevices following the methods of Lagally et al. [38,11,39] and the development of complete microfabricated chemical analysis systems for extraterrestrial exploration [41].

Acknowledgements

Device fabrication was performed at the University of California, Berkeley Microfabrication Laboratory. This research was supported by the Director, Office of Science, Office of Biological and Environmental Research of the US Department of Energy under Contract DEFG91ER61125. AMS is supported by NASA grant NAG5-9659. ETL gratefully acknowledges the support of a Whitaker Foundation Predoctoral Fellowship.

References

[1] D.J. Harrison, K. Fluri, K. Seiler, Z. Fan, C.S. Effenhauser, A. Manz, Micromachining a miniaturized capillary electrophoresis-based chemical analysis system on a chip, Science 261 (1993) 895–897.

[2] J.M. Ramsey, A. van den Berg (Eds.), Proceedings of the MicroTAS 2001 Symposium, Monterey, CA, USA, October 21–25, 2001, Kluwer Academic Publishers, Dordrecht, The Netherlands.

[3] D.R. Reyes, D. Iossifidis, P.-A. Auroux, A. Manz, Micro total analysis systems. 1. Introduction, theory, and technology, Anal. Chem. 74 (2002) 2623–2636.

[4] H. Tian, A. Jaquins-Gerstl, N. Munro, M. Trucco, L.C. Brody, J.P. Landers, Single-strand conformation polymorphism analysis by capillary and microchip electrophoresis: a fast, simple method for detection of common mutations in BRCA1 and BRCA2, Genomics 63 (2000) 25–34.

[5] M.C. Mitchell, V. Spikmans, A. Manz, A.J. de Mello, Microchip-based synthesis and total analysis systems (μSYNTAS): chemical microprocessing for generation and analysis of compound libraries, J. Chem. Soc., Perkin Trans. 1 (2001) 514–518.

[6] I. Medintz, W.W. Wong, L. Berti, L. Shiow, J. Tom, J. Scherer, G. Sensabaugh, R.A. Mathies, High-performance multiplex SNP analysis of three hemochromatosis-related mutations with capillary array electrophoresis microplates, Genome Res. 11 (2001) 413–421.

[7] B.M. Paegel, C.A. Emrich, G.J. Wedemayer, J.R. Scherer, R.A. Mathies, High throughput DNA sequencing with a microfabricated 96-lane capillary array electrophoresis bioprocessor, Proc. Natl. Acad. Sci. USA 99 (2002) 574–579.

[8] M.J. Powers, K. Domansky, M.R. Kaazempur-Mofrad, A. Kalezi, A. Capitano, A. Upadhyaya, P. Kurzawski, K.E. Wack, D.B. Stolz, R. Kamm, L.G. Griffith, A microfabricated array bioreactor for perfused 3D liver culture, Biotechnol. Bioeng. 78 (2002) 257–269.

[9] L.D. Hutt, D.P. Glavin, J.L. Bada, R.A. Mathies, Microfabricated capillary electrophoresis amino acid chirality analyzer for extraterrestrial exploration, Anal. Chem. 71 (1999) 4000–4006.

[10] R.C. Anderson, X. Su, G.J. Bogdan, J. Fenton, A miniature integrated device for automated multistep genetic assays, Nucl. Acids Res. 28 (2000) e60.

[11] E.T. Lagally, C.A. Emrich, R.A. Mathies, Fully integrated PCR-capillary electrophoresis microsystem for DNA analysis, Lab on a Chip 1 (2001) 102–107.

[12] L. Bousse, S. Mouradian, A. Minalla, H. Yee, K. Williams, R. Dubrow, Protein sizing on a microchip, Anal. Chem. 73 (2001) 1207–1212.

[13] M.T. Taylor, P. Belgrader, R. Joshi, G.A. Kintz, M.A. Northrup, Fully automated sample preparation for pathogen detection performed in a microfluidic cassette, in: Proceedings of the Micro Total Analysis Systems, Monterey, CA, USA, 2001, pp. 670–672.

[14] H.T.G. van Lintel, F.C.M. van de Pol, S. Bouwstra, A piezoelectric micropump based on micromachining of silicon, Sens. Actuat. 15 (1988) 153–167.

[15] T.T. Veenstra, J.W. Berenschot, J.G.E. Gardeniers, R.G.P. Sanders, M.C. Elwenspoek, A. van den Berg, Use of selective anodic bonding to create micropump chambers with virtually no dead volume, J. Electrochem. Soc. 148 (2001) G68–G72.

[16] D.L. Smith, Thin-film Deposition: Principles and Practice, McGraw-Hill, New York, 1995.

[17] C. Vieider, O. Ohman, H. Elderstig, A pneumatically actuated micro valve with a silicone rubber membrane for integration with fluid-handling systems, in: Proceedings of the Eighth International Conference on Solid-State Sensors and Actuators, and Eurosensors IX, Stockholm, Sweden, 1995, pp. 284–286.

[18] L. Bousse, E. Dijkstra, O. Guenat, High-density arrays of valves and interconnects for liquid switching, in: Proceedings of the Solid-State Sensor and Actuator Workshop, Hilton Head Island, SC, USA, 1996, pp. 272–275.

[19] T. Ohori, S. Shoji, K. Miura, A. Yotsumoto, Partly disposable three-way microvalve for a medical micro total analysis system (μTAS), Sens. Actuat. A 64 (1998) 57–62.

[20] X. Yang, C. Grosjean, Y.-C. Tai, C.-M. Ho, A MEMS thermopneumatic silicone rubber membrane valve, Sens. Actuat. A 64 (1998) 101–108.

[21] D. Baechi, R. Buser, J. Dual, A high density microchannel network with integrated valves and photodiodes, Sens. Actuat. A 95 (2002) 77–83.

[22] S. Sjolander, C. Urbaniczky, Integrated fluid handling system for biomolecular interaction analysis, Anal. Chem. 63 (1991) 2338–2345.

[23] S. Bohm, W. Olthuis, P. Bergveld, A plastic micropump constructed with conventional techniques and materials, Sens. Actuat. A 77 (1999) 223–228.

[24] W.K. Schomburg, R. Ahrens, W. Bacher, J. Martin, V. Saile, AMANDA—surface micromachining, molding, and diaphragm transfer, Sens. Actuat. A 76 (1999) 343–348.

[25] Y. Xia, G.M. Whitesides, Soft lithography, Annu. Rev. Mater. Sci. 28 (1998) 153–184.

[26] K. Hosokawa, R. Maeda, A pneumatically-actuated three-way microvalve fabricated with polydimethylsiloxane using the membrane transfer technique, J. Micromech. Microeng. 10 (2000) 415–420.

[27] M.A. Unger, H.-P. Chou, T. Thorsen, A. Scherer, S.R. Quake, Monolithic microfabricated valves and pumps by multilayer soft lithography, Science 288 (2000) 113–116.

[28] X.Q. Ren, M. Bachman, C. Sims, G.P. Li, N. Allbritton, Electroosmotic properties of microfluidic channels composed of poly-(dimethylsiloxane), J. Chromatogr. B 762 (2001) 117–125.

[29] S. Hu, X. Ren, M. Bachman, C.E. Sims, G.P. Li, N. Allbritton, Surface modification of poly(dimethylsiloxane) microfluidic devices by ultraviolet polymer grafting, Anal. Chem. 74 (2002) 4117–4123.

[30] C.S. Effenhauser, G.J.M. Bruin, A. Paulus, M. Ehrat, Integrated capillary electrophoresis on flexible silicone microdevices: analysis of DNA restriction fragments and detection of single DNA molecules on microchips, Anal. Chem. 69 (1997) 3451–3457.

[31] J.W. Hong, T. Fujii, M. Seki, T. Yamamoto, I. Endo, Integration of gene amplification and capillary gel electrophoresis on a polydimethylsiloxane-glass hybrid microchip, Electrophoresis 22 (2001) 328–333.

[32] D.J. Harrison, K. Fluri, N. Chiem, T. Tang, Z. Fan, Micromachining chemical and biochemical analysis and reaction systems on glass substrates, Sens. Actuat. B 33 (1996) 105–109.

[33] J.P. Alarie, S.C. Jacobson, B.S. Broyles, T.E. McKnight, C.T. Culbertson, J.M. Ramsey, Electroosmotically induced hydraulic pumping on microchips, in: Proceedings of the Micro Total Analysis Systems, Monterey, CA, USA, 2001, pp. 131–132.

[34] S. Zeng, C.-H. Chen, J.G. Santiago, J.-R. Chen, R.N. Zare, J.A. Tripp, F. Svec, J.M.J. Frechet, Electroosmotic flow pumps with polymer frits, Sens. Actuat. B 82 (2002) 209–212.

[35] P. van der voort, E.F. Vansant, Silylation of the silica surface: a review, J. Liq. Chromatogr. Relat. Technol. 19 (1996) 2723–2752.

[36] P.C. Simpson, A.T. Woolley, R.A. Mathies, Microfabrication technology for the production of capillary array electrophoresis chips, Biomed. Microdevices 1 (1998) 7–26.

[37] E.T. Lagally, B.M. Paegel, R.A. Mathies, Microfabrication technology for chemical and biochemical microprocessors, in: Proceedings of the Micro Total Analysis Systems, Enschede, The Netherlands, 2000, pp. 217–220.

[38] E.T. Lagally, P.C. Simpson, R.A. Mathies, Monolithic integrated microfluidic DNA amplification and capillary electrophoresis analysis system, Sens. Actuat. B 63 (2000) 138–146.

[39] E.T. Lagally, I. Medintz, R.A. Mathies, Single-molecule DNA amplification and analysis in an integrated microfluidic device, Anal. Chem. 73 (2001) 565–570.

[40] R.A. Mathies, E.T. Lagally, T. Kamei, W.H. Grover, C.N. Liu, J.R. Scherer, Capillary array electrophoresis bioprocessors, in: Proceedings of the Solid-State Sensor, Actuator and Microsystems Workshop, Hilton Head Island, SC, USA, June 2–6, 2002, pp. 112–117.

[41] A.M. Skelley, R.A. Mathies, J.L. Bada, F.J. Grunthaner, Mars Organic Detector III: a versatile instrument for detection of bio-organic signatures on Mars, in: Proceedings of the International Society for Optical Engineering (SPIE), In Situ Instrument Technologies Workshop, Pasadena, CA, in press.